Levels in ^{99}Ru populated by the (^{3}He,2nγ) reaction: Complete particle-core multiplets

C. S. Whisnant,* K. D. Carnes,† R. H. Castain,‡ F. A. Rickey, G. S. Samudra, and P. C. Simms
Tandem Accelerator Laboratory, Purdue University, Lafayette, Indiana 47907
(Received 20 May 1985)

The energy-level structure of ^{99}Ru was studied using the ^{98}Mo(^{3}He, 2nγ)^{99}Ru reaction at a bombarding energy of 13 MeV, in an attempt to populate an extensive set of non-yrast states. The experiments included γ-ray excitation functions, γ-γ coincidence measurements, γ-ray angular distributions, and γ-ray linear polarization measurements. A large number of non-yrast states were observed, with angular momenta ranging from $\frac{1}{2}$ to $\frac{17}{2}$. The comparison of experimental energies and electromagnetic transition properties to the predictions of a particle-rotor model is presented. This interpretation suggests that several complete particle-core multiplets have been populated. The population of non-yrast states is attributable to the properties of the reaction rather than any details of the nuclear structure involved.

I. INTRODUCTION

One of the most useful tools for the study of collective nuclear properties is the (HI,xnγ) reaction. The band structures observed in odd-A nuclei following these reactions have been investigated extensively and have facilitated the development of many collective descriptions. The heavy-ion data, however, are not sufficient for the selection of a preferred model. The band structures observed, for example in the transitional nuclei, are yrast states which represent only a small fraction of the states predicted by any of the various models. Light-ion-induced reactions can populate non-yrast states, but each naturally has its own selection rules which pick out a different sub-set of the states present. A reaction which can systematically populate a more complete set of non-yrast states is desirable.

It is possible to populate non-yrast states with a wide range of angular momenta by using the (^{3}He,2nγ) reaction at bombarding energies near the Coulomb barrier. The ^{3}He projectile has been chosen because of its large mass excess. As a specific test of this approach a ^{98}Mo target has been bombarded to populate states in ^{99}Ru. In a preliminary report of this work,[1] evidence for the population of several complete particle-core multiplets was presented. This paper contains a more extensive description of the work. Specific problems presented by the ^{3}He projectile, and solutions to them, will be discussed. A particle-rotor model will be used to examine the completeness of the reactions.

II. PROPERTIES OF THE REACTION

The dominant property of most (HI,xnγ) reactions is the formation of a compound nucleus at both high energy and high angular momentum. The evaporated neutrons carry away little angular momentum. The residual nucleus then normally emits several high energy dipole transitions. All of these radiations result in a relatively small decrease in angular momentum, thus the yrast line is quickly reached. In order to populate a substantial set of non-yrast states the angular momentum in the residual nucleus must be reduced while maintaining a high initial excitation energy E_0. The excitation energy is important for two reasons. The level density is high, and the formation of the residual nucleus involves many states. Thus spectroscopic selection rules are averaged out in the resultant gamma decay. The energy dependence of the dipole radiation is also minimized. The maximum possible decay energy, E_γ, is the difference between the initial excitation energy E_0 and the yrast energy for the appropriate angular momentum. The non-yrast states of interest lie in some energy range ΔE above the yrast line. As long as ΔE is small compared to E_γ, transition rates to all these states can be similar. For a given projectile the angular momentum of the compound system can be reduced by lowering the incident energy relative to the Coulomb barrier. This, however, reduces the excitation energy, and the yrast line is again reached. Lighter projectiles are accompanied by lower Coulomb barriers, hence lower excitation energies are usually achieved. However, the desired excitation energy could be maintained as the bombarding energy is decreased if one could increase the Q-value of the reactions. This hypothetical situation can be approximated by choosing a reaction whose Q-value is abnormally high. The large mass excess of the ^{3}He results in higher Q-values for (^{3}He,xnγ) reactions than for any other viable choices. With this projectile the combination of low angular momentum and high excitation energies can be achieved by employing incident energies just above the Coulomb barrier. These conditions have been utilized in the present work.

The nuclear orientation obtained in (^{3}He,xnγ) reactions is smaller than that achieved in (HI,xnγ) reactions. Thus angular distributions of emitted radiation in the former case are attenuated relative to those in the latter. Spin assignments are therefore more difficult. The combination of angular distribution and linear polarization measurements can minimize this problem, as will be discussed later. Yrast arguments can no longer be used in making

spin assignments. The quantitative analysis of excitation functions allows distinction between $\pm|\Delta I|$ spin changes. Break-up of the ^{3}He projectile in the Coulomb field of the target also creates problems. When the projectile breaks up, compound Tc nuclei can be formed by capture of a break-up product. Since this process substantially competes with ^{3}He capture at the low incident energies employed here, many of the γ-transitions detected were from ^{99}Tc. We have developed a large-solid-angle charged-particle detector which, when operated in coincidence with a γ-ray detector, identifies these transitions. This system will be described subsequently.

III. EXPERIMENTAL PROCEDURES

The measurements performed in this work included excitation functions, sorting of γ-rays by coincidence with charged particles emitted, γ-ray angular distributions, γ-ray linear polarizations, and γ-γ coincidences.

The target used in these experiments was a foil of isotopically separated ^{98}Mo, rolled to a uniform thickness of 1.8 mg/cm^2. To prevent Doppler shifting of the radiations emitted as the residual nucleus recoils, a thin layer of ^{197}Au was evaporated on the back of the target. The 1.5 mg/cm^2 layer was sufficient to stop all recoiling nuclei and eliminate the Doppler shifting of all but the fastest transitions.

This thin Au backing was not sufficient to stop the beam. To facilitate measurements at zero degrees, a thick piece of Au was sandwiched behind the target. Since the range of ^{3}He is approximately 50 mg/cm^2 at 20 MeV, the 58 mg/cm^2 backing was enough to completely arrest the beam at the energies used.

The ^{3}He beam currents of 5 to 10 nA used in these experiments were supplied by the Purdue FN tandem Van de Graaff accelerator.

The three Ge(Li) detectors used in these measurements have resolutions ranging from 1.9 to 2.1 keV at 1332 keV and nominal volumes of 50 cm^3.

The gain and zero level of the detector-electronics system are monitored during a singles experiment using the Coulomb excitation lines from the gold backing (191.5, 268.71, 278.91, and 547.62 keV) and a ^{60}Co source placed near the detector (1173.23 and 1332.48 keV). From the use of these internal standards, the energy of a relatively intense, clean γ-ray could be measured with an accuracy of approximately 50 eV. Keeping an accurate track of energy calibrations during a coincidence experiment is more difficult, as only gamma rays from the target are seen. While it is useful to monitor the Coulomb excitation lines of the ^{98}Mo, these lines are weak and often obscured by other gamma rays. The only reasonable solution was to check and reset the energy calibration off-line frequently.

Careful energy calibrations are done off-line with a ^{182}Ta-^{152}Eu radioactive source. There are about 65 strong lines ranging from 65 keV to 1408 keV, making this a useful source for this purpose. The energies of these radiations have previously been determined to within $\pm$0.1 keV. To account for nonlinearities in the detector-electronics system, the energy is determined from a least squares fit to the Ta-Eu data.

A. Excitation functions

Excitation functions were measured over the range of 10 to 14 MeV since rough calculations indicated that the Coulomb barrier for ^{3}He on ^{98}Mo was $\sim$12 MeV. These measurements serve as both a basis for choosing the bombarding energy for subsequent measurements and for spin determination.

Gamma rays from reactions producing ^{99}Ru, ^{99}Tc, and ^{98}Ru were seen to dominate the observed spectra. The production of ^{99}Tc was seen to dominate at all energies. On the basis of Q-values, the 2n reaction should dominate the pn reaction. Break-up of the ^{3}He projectile can, however, produce Tc directly due to deuteron or proton capture, simulating pn or p2n reaction. The dominance of the "pn" reaction seems to indicate that break-up is very probable at the low incident energies employed here. The resulting problem of identifying the large number of transitions accompanied by charged-particle emission will be discussed below.

A bombarding energy of 13 MeV represents a compromise between the relative intensities of the 2n and 3n channels. Although the excitation function of any individual transition has an overall energy dependence characteristic of the reaction channel, the detailed energy dependence is sensitive to the angular momentum of the initial state. Details of the analysis will be presented in Sec. IV.

B. Charged particle detection

Excitation functions do not provide satisfactory identification of the reaction channel involved. Crudely speaking, reaction channels with the same number of exit particles, i.e., 2n and pn, have a similar energy dependence. Particle-identification schemes can completely label the emitted particles, but the small solid-angles involved limit the counting rate. However, in many cases, such as the present work, the knowledge that one of the emitted particles is charged is valuable. We have constructed a large solid-angle charged-particle detection system which accomplishes this desire. Details of the system will be described elsewhere.[2] The detectors are two thin discs of plastic scintillator (NE100) coupled to RCA 8575 phototubes by Lucite light pipes. The scintillator thickness of 0.5 mm was chosen to minimize sensitivity to γ-rays and neutrons while providing adequate efficiency for proton detection. (The range of a 6 MeV proton in NE100 is 0.5 mm.) Lead absorbers were attached to each assembly to shield the scintillators from scattered ^{3}He and emitted α particles. The diameter of each scintillator was 4.45 cm, matching the light sensitive surface of the phototube. The two assemblies actually formed the top and bottom surface of the scattering chamber, positioning each scintillator 0.79 cm from target center. This resulted in a total solid angle of 66.4% for the system. The detectors have no energy sensitivity, but are very fast, making them ideal for tagging γ-rays emitted in coincidence with charged particles.

In the present work this system was used in a singles measurement to help identify ^{99}Ru γ-rays. Gamma rays were sorted into two spectra on the basis of coincident signals from the scintillators. The gated, or "proton," spec-

trum contained only lines for which an emitted proton was detected in coincidence. Known transitions in ^{99}Tc were present, and no known ^{99}Ru transitions were found. The "neutron" spectrum, defined as the total minus the gated spectrum, contained all of the transitions from the "proton" spectrum at reduced intensities. Ratios of gated to total intensities were used to determine the sorting efficiency of the system. This was found to be approximately 40%, less than the solid angle due to the angular distribution of emitted protons. Smaller sorting efficiencies can indicate doublets. This information is included in Table II.

C. Angular distributions

The angular distribution measurements consisted of singles spectra collected at nine evenly spaced angles from $+90°$ to $-30°$ with respect to the beam axis. The measurements were used not only as a primary part of spin change and mixing ratio determinations, but to determine energies and intensities of γ-rays. A typical spectrum is seen in Fig. 1.

On-demand beam pulsing was utilized in these measurements. Every time a γ-ray was detected the beam was swept off the target by electrostatic deflectors and held off the target until the γ-ray pulse had been processed. This technique reduced pileup, resulting in a 50% increase in the through-put rate of useful data and a reduction in background. Neutron damage to the detector was substantially reduced. Normalization of the data was more complicated than in direct current measurements, since the probability of pileup is no longer constant over the duration of the bombardment. Simplistically a pulser was injected into the system, and the number of pulses presented while the beam was on target was compared to the number of pulses accepted. Along with other small corrections, this ratio was used to correct the live charge. Care must be taken to ensure that the pulser signal is treated just as any in-beam γ-ray.

D. Linear polarizations

The γ-ray linear polarizations were obtained by measuring γ-ray Compton scattering in directions parallel and

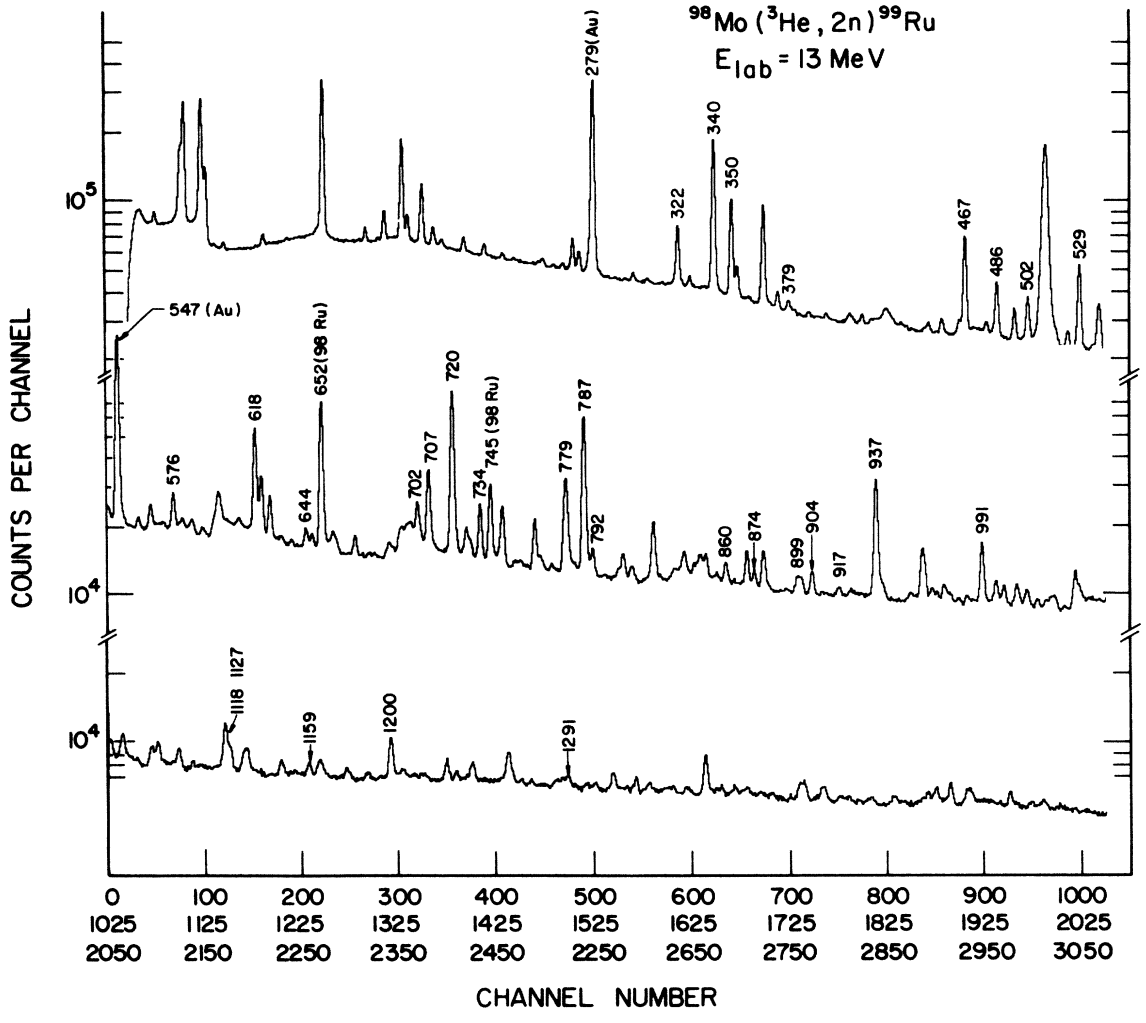

FIG. 1. Singles spectrum from the ^{98}Mo(^{3}He,2nγ) ^{99}Ru reaction.

perpendicular to the beam direction. In terms of these quantities the polarization is

$$P_\gamma = \frac{1}{Q}\frac{N(90°)-N(0°)}{N(90°)+N(0°)} . \quad (1)$$

Q is the efficiency of the polarimeter as determined from data taken for γ-rays of known polarizations. The polarimeter consists of two conventional Ge(Li) detectors placed on a turntable below the target, and has been described previously.[3] On demand beam pulsing was again employed, with the beam pulser being triggered by either detector. The coincidence-polarization data were normalized by singles data taken simultaneously.

E. γ-γ coincidence measurement

The three-detector coincidence measurements followed techniques described previously.[4] The detectors were positioned at $+100°$, $0°$, and $-100°$. On demand beam pulsing was again used, with the requirement that a pair of detectors fired before the beam was removed from the target. No normalization was required.

IV. ANGULAR MOMENTUM ANALYSIS

In the normal (HI,xnγ) reaction, the final nucleus is highly oriented. Thus the analysis of angular distributions can often identify spin charges, since the relevant angular distribution coefficients can be measured with sufficient accuracy. This is not the case for the (^{3}He,2nγ) reaction discussed here.

The angular distribution of γ-radiation emitted from an oriented state can be described as[5]

$$W(\theta) = 1 + Q_2 A_{22}(\gamma) P_2(\cos\theta) + Q_4 A_{44}(\gamma) P_4(\cos\theta) , \quad (2)$$

where the Q_k are solid angle correction factors[6] and the P_k are Legendre polynomials. The angular distribution coefficients $A_{kk}(\gamma)$ can be expressed as the product of orientation parameters $B_k(I_i)$ which describe the alignment of the initial state and distribution coefficients $A_k(\lambda)$ which are characterized by the initial spin, the change in angular momentum, and the multipole nature of the transition.

$$A_{kk}(\gamma) = B_k(I_i) A_k(\gamma) . \quad (3)$$

In terms of the relative populations $P(m)$ of the $|I_i m\rangle$ substates the $B_k(I_i)$ are

$$B_k(I) = (2I+1)^{1/2} \sum_{m=-I}^{I} (-1)^{I+m} \langle I -m I m \mid k 0 \rangle P(m) , \quad (4)$$

and for a mixed L and L' transition

$$A_k(\gamma) = \frac{F_k(LLI_fI) + 2\delta F_k(LL'I_fI) + \delta^2 F_k(L'L'I_fI)}{1+\delta^2} , \quad (5)$$

where δ is the mixing ratio in the convention of Krane and Steffen,[7] and the F_k are standard F coefficients. The $B_k(I)$ for maximum alignment, $B_k^0(I)$, are readily calculated, and it is convenient to define attenuation coefficients α_k which relate the actual orientation parameters to the $B_k^0(I)$

$$\alpha_k = \frac{B_k(I)}{B_k^0(I)} . \quad (6)$$

For mixed transitions there are thus three unknowns (α_2, α_4, and δ) but at most only two observables (A_{22} and A_{44}), which presents a fundamental problem. When there are enough unmixed transitions (E2's for example) observed, the α_k for many states can be directly measured. It is then possible to calculate the α_k for nearby states using calculated deorientation coefficients. In the present work this is impractical due to the small number of pure transitions. However the α_2 and α_4 can be related using an approximate model for $P(m)$:[5]

$$P(m) = \frac{\exp\left[-\frac{m^2}{2\sigma^2}\right]}{\sum_{m'=-I}^{I} \exp\left[-\frac{m'^2}{2\sigma^2}\right]} . \quad (7)$$

This model reproduces the trends of the α_2–α_4 relationships where they are known (pure multipoles) although the α_4 values tend to be 20–30 % too low. It has the enormous value of eliminating a parameter, reducing the number of unknown to two, σ and δ. The model shows that as σ increases, α_4 decreases much faster than α_2. For example, an α_2 of 0.8 corresponds to an α_4 of $\sim$0.48, while an α_2 of 0.4 corresponds to an α_4 of $\sim$0.08.

Thus, a typical A_{44}, which could be clearly measured in the former case (i.e., $A_{44} = -0.114 \pm 0.030$), becomes consistent with zero in the latter case. This illustrates the dilemma found when the nuclear system is relatively deoriented: the emitted γ-radiations have angular distributions which are sensitive to the A_{22} values only. This makes it impossible to uniquely determine spin changes in many cases.

Linear polarization measurements have been widely utilized to identify parity-changing transitions. These measurements can also be a powerful tool in identifying the spin change involved.

The linear polarization (P_γ) at 90° to the beam may be defined as[8]

$$P_\gamma = \frac{I(0°)-I(90°)}{I(0°)+I(90°)} , \quad (8)$$

where $I(0°)$ and $I(90°)$ are the intensities of γ radiation with electric vectors parallel and perpendicular, respectively, to the beam direction. This polarization can be expressed in terms of the *measured* angular distribution coefficients for the transition

$$P_\gamma = \pm \frac{3A_{22}H_2(\delta) + 1.25A_{44}H_4(\delta)}{2 - A_{22} + 0.75A_{44}} \begin{cases} +\text{no parity change} \\ -\text{parity change} \end{cases} \quad (9)$$

The $H_k(\delta)$ are given in terms of the same F-coefficient as the A_{kk}.[9]

$$H_2(\delta)=\frac{F_2(LLI_fI)-2/3\delta F_2(LL'I_fI)+\delta^2F_2(L'L'I_fI)}{F_2(LLI_fI)+2\delta F_2(LL'I_fI)+\delta^2F_2(L'L'I_fI)}\ , \tag{10}$$

and

$$H_4(\delta)=1\ . \tag{11}$$

The A_{22} and $H_2(\delta)$ have a common factor so that

$$A_{22}H_2(\delta)=\alpha_2B_2^0(I)\left[\frac{F_2(LLI_fI)-2/3\delta F_2(LL'I_fI)+\delta^2F_2(L'L'I_fI)}{1+\delta^2}\right] \tag{12}$$

$$\equiv\alpha_2B_2^0(I)G_2(\delta) \tag{13}$$

If the A_{44} are severely attenuated, the expression for P_γ becomes approximately

$$P_\gamma\sim\pm\frac{3\alpha_2B_2^0(I)G_2(\delta)}{2-A_{22}}\ . \tag{14}$$

It is seen from Eqs. (5) and (12) that P_γ and $A_2(\gamma)$ depend on exactly the same quantities, but the sign of the linear term in the mixing ratio is different. Figures 2 and 3 show P_γ and $A_2(\gamma)$ as a function of δ for typical $\Delta I=-1$ and $\Delta I=0$ transitions. The value of the dual $A_{22}(\gamma)$–P_γ measurement is evident. A $\Delta I=-1$ transition with an E2/M1 mixing ratio around $\delta=+1$ can have a large positive A_2, but must have a large negative P_γ. On the other hand, a $\Delta I=0$ transition (again E2/M1) with a large positive A_2 must have a positive P_γ. The same attenuation parameter, α_2, dominates both the $A_{22}(\gamma)$ and the P_γ, and in fact the ratio is independent of the orientation. Thus, mixing ratios can be extracted in a straightforward fashion.

In our work we utilize the combined angular distribution and linear polarization measurements in the following manner. Initially, the angular distribution data are processed in the standard way to obtain A_{22} values and A_{44} values for each transition. These coefficients are used to suggest possible spin changes and to check the results of further analysis. The extracted coefficients could be directly compared with the measured P_γ. However, the uncertainties in the A_{kk} are correlated, and we have elected to follow another procedure. A trial spin change is specified. In order to estimate a starting value for the parameters σ and δ, we assume that A_4 is zero. We then calculate an anisotropy from the angular distribution data, and extract a tentative A_{22}. The measured P_γ is corrected, using this estimated A_{22}, to yield a number which depends only on α_2 and $G_2(\delta)$.

$$\frac{2-A_{22}}{3}P_\gamma=\pm\alpha_2B_2^0(I)G_2(\delta)\ . \tag{15}$$

The measured A_{22} are typically in the range from $+0.3$ to -0.6. Thus, uncertainties in A_{22} are not a major problem. Using tabulated F-coefficients and calculated $B_2^0(I)$ values in this expression and the corresponding equation for A_{22}, values for α_2 and δ are extracted. If the wrong spin change has been specified, unphysical values may be obtained, and the assignment is rejected. If the results are physically meaningful, they are used as starting values in a grid search. The Gaussian model for $P(m)$ is used so that the parameters in the grid are σ and δ. At each point in the grid, both a theoretical angular distribution and P_γ are calculated, including contributions from the A_{44} term. The agreement with the data is evaluated by calculating an error weighted chi-square. The "best" values of σ and δ are assumed to be those which minimize chi-square. If several spin changes are tested, the relative chi-squares are

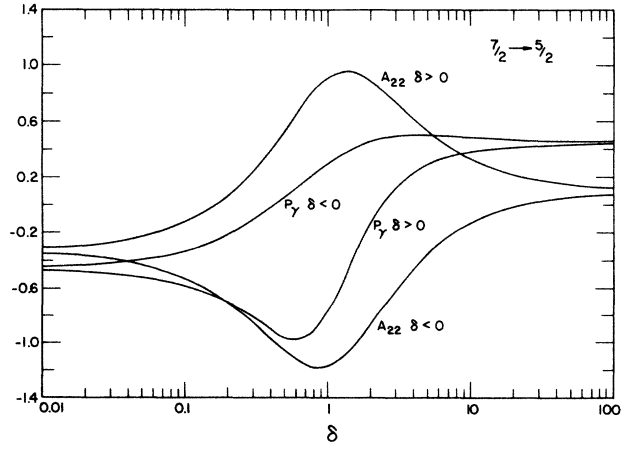

FIG. 2. Dependence of the angular distribution coefficient A_{22} and the linear polarization P_γ on the multipole mixing ratio δ for a typical $\Delta I=-1$ transition.

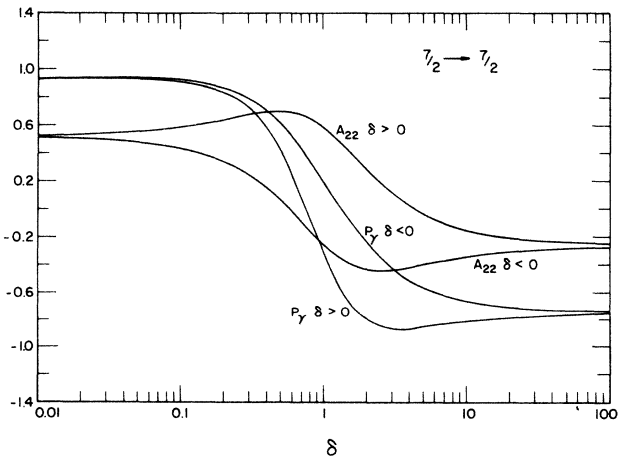

FIG. 3. Dependence of the angular distribution coefficient A_{22} and the linear polarization P_γ on the multipole mixing ratio δ for a typical $\Delta I=0$ transition.

used to indicate the most probable one. For this spin change, limits on σ and δ are assigned by locating the contour where chi-square is double the minimum, or two if the minimum is less than one.

There remain ambiguities. For example pure $\Delta I=0$ and $\Delta I=2$ transitions are sometimes difficult to distinguish. Of greater significance is the insensitivity of the angular-distribution-polarization analysis to the sign of ΔI. In (HI,xnγ) reactions the same situation is found, but yrast arguments make spin increases highly improbable. In the present work these arguments cannot be used. A quantitative analysis of excitation functions yields valuable spin information to resolve these ambiguities.

As the bombarding energy increases, so does the angular momentum carried into the system. Thus there is a systematic trend to increase the population of higher spin states relative to those of lower spin, which is reflected in excitation functions. When long cascades are present this effect is not very useful. In the case of light-ion-induced reactions excitation functions can be a more specific measure of spin. Following previously published procedures,[10] we have first removed the predominate energy dependence of the reaction by normalizing all excitation functions of interest to that of the 341-keV transition depopulating the known $\frac{7}{2}^+$ state at 341 keV. It has been observed that the normalized excitation function of each transition is an exponential function of energy. The logs of the intensities can thus be fit linearly, and the slopes of the lines compared to slopes for known initial spins. Figure 4 shows the normalized functions for six transitions from states of known spin. The slopes are quite distinctive, and indicate that the basic technique may be used to measure unknown spins with reasonable certainty. In practice, when slopes and uncertainties for all transitions of interest were determined, it was observed that distinct grouping around the slopes of Fig.4 were obtained. We imply from this that in general excitation functions can reduce the possible spin assignment for a state to two values, and with favorable statistics can produce a unique assignment. This is all phenomenological, but when excitation functions are used in conjunction with the angular distribution-polarization analysis, rather convincing spin assignments may be obtained.

Table I illustrates the combined angular-momentum analysis for three transitions selected because their angular distributions were nondescript. They all have positive A_{22} values (and statistically zero A_{44} values) which would allow $\Delta I=\pm2,\pm1$, or 0 spin changes. The angular-distribution-polarization analysis partially resolves the problem. For the 791.89-keV transition $\Delta I=\pm2$ or 0 is ruled out, but $\Delta I=-1$ is only slightly preferred over $\Delta I=+1$. For the 648.0-keV transition $\Delta I=\pm1$ is preferred, with $\Delta I=0$ possible. For the 702.0-keV transition both $\Delta I=0$ and $\Delta I=\pm2$ are possibilities. Inclusion of the excitation functions analysis removes the ambiguities. In the first case the excitation function prefers $I_i=\frac{13}{2}$ with $\frac{11}{2}$ possible, which eliminates the $\Delta I=+1$ possibility. In the second case a strong preference for $I_i=\frac{9}{2}$ was found, indicating that $\Delta I=+1$ is the correct assignment. In the last case I_i could be either $\frac{9}{2}$ or $\frac{11}{2}$, but not $\frac{7}{2}$. Thus a $\Delta I=-2$ assignment is required. In all cases the excitation function analysis was found to be consistent with the angular-distribution-polarization results, establishing some confidence in the technique. Therefore in a few cases where no useful angular distribution-polarization-analysis was available tentative spins have been assigned based solely on excitation functions.

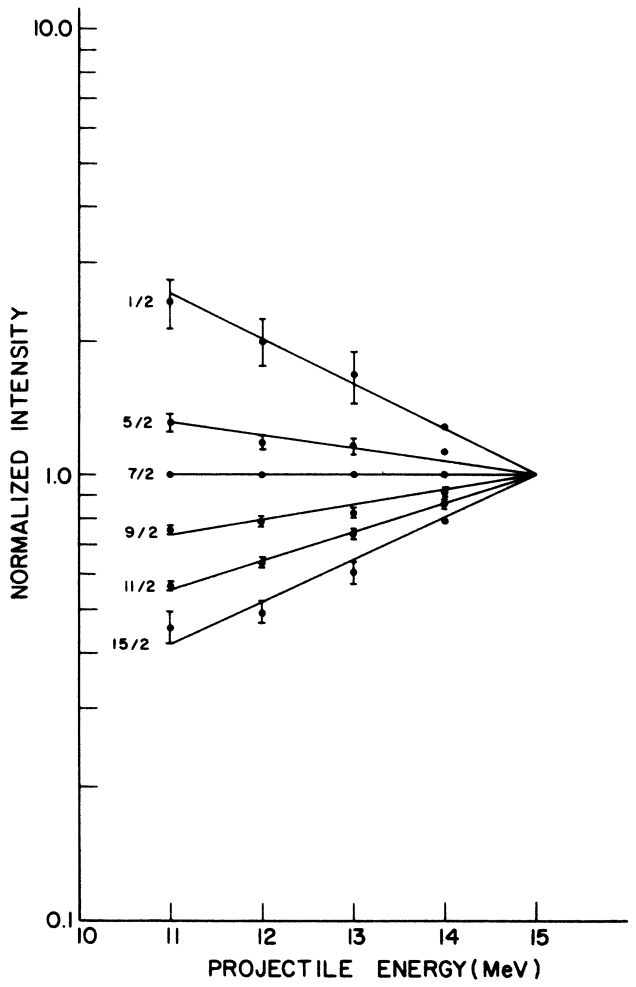

FIG. 4. Relative excitation functions for a few known transitions in ^{99}Ru.

A separate aspect of the angular momentum analysis was based on DCOQ (directional correlation from oriented nuclei referred to quadrupole transitions) ratios extracted from the coincidence data. This technique has been described previously.[11] When a transition is contaminated in singles measurements, the DCOQ ratios are often the only information concerning spin changes. When the orientation of the nucleus is small, however, DCOQ ratios can play a more general role. The nuclear orientation of the initial state is involved, although it appears in both numerator and denominator so that the magnitude is not attenuated linearly with the decrease in orientation. After emission of the first γ ray in a given direction, the directional correlation of subsequent emission is less sensitive to the beam produced orientation. Thus there are cases where the measured DCOQ can resolve ambiguities present in the angular distribution and polarization

TABLE I. Example of detailed angular momentum analysis

E_γ (keV)	A_{22} (Expt)	P_γ (Expt)	$I_i > I_f$	A_{22} (Theor)	P_γ (Theor)	χ^2	δ	α_2	I_i (Ex. func)
791.89	0.35(0.05)	−0.7(0.2)	$\frac{15}{2} \rightarrow \frac{11}{2}$	0.11	0.17	81	0	0.72	
			$\frac{13}{2} \rightarrow \frac{11}{2}$	0.41	−0.78	0.7	0.39	0.9	
			$\frac{11}{2} \rightarrow \frac{11}{2}$	0.28	−0.28	43	1.1	0.85	$\frac{13}{2}$,($\frac{11}{2}$)
			$\frac{9}{2} \rightarrow \frac{11}{2}$	0.42	−0.7	1.8	−1.8	0.93	
			$\frac{7}{2} \rightarrow \frac{11}{2}$	0.12	0.2	81	0	0.56	
648.0	0.28(0.15)	−0.16(0.14)	$\frac{15}{2} \rightarrow \frac{11}{2}$	0.05	0.07	6.4	0	0.1	
			$\frac{13}{2} \rightarrow \frac{11}{2}$	0.13	−0.30	0.2	0.32	0.41	
			$\frac{11}{2} \rightarrow \frac{11}{2}$	0.013	−0.05	1.6	2.0	0.5	$\frac{9}{2}$,($\frac{11}{2}$)
			$\frac{9}{2} \rightarrow \frac{11}{2}$	0.12	−0.17	0.2	−0.22	0.6	
			$\frac{7}{2} \rightarrow \frac{11}{2}$	0.04	0.07	6.3	0	0.18	
702.0	0.05(0.03)	0.15(0.1)	$\frac{11}{2} \rightarrow \frac{7}{2}$	0.07	0.16	1.6	0	0.24	
			$\frac{9}{2} \rightarrow \frac{7}{2}$	0.02	0.004	6	21	0.2	
			$\frac{7}{2} \rightarrow \frac{7}{2}$	0.06	0.14	1.3	−0.15	0.19	$\frac{9}{2}$, $\frac{11}{2}$
			$\frac{5}{2} \rightarrow \frac{7}{2}$	0.03	−0.08	9.5	−0.2	0.2	
			$\frac{3}{2} \rightarrow \frac{7}{2}$	0.10	0.16	1.7	0	0.7	

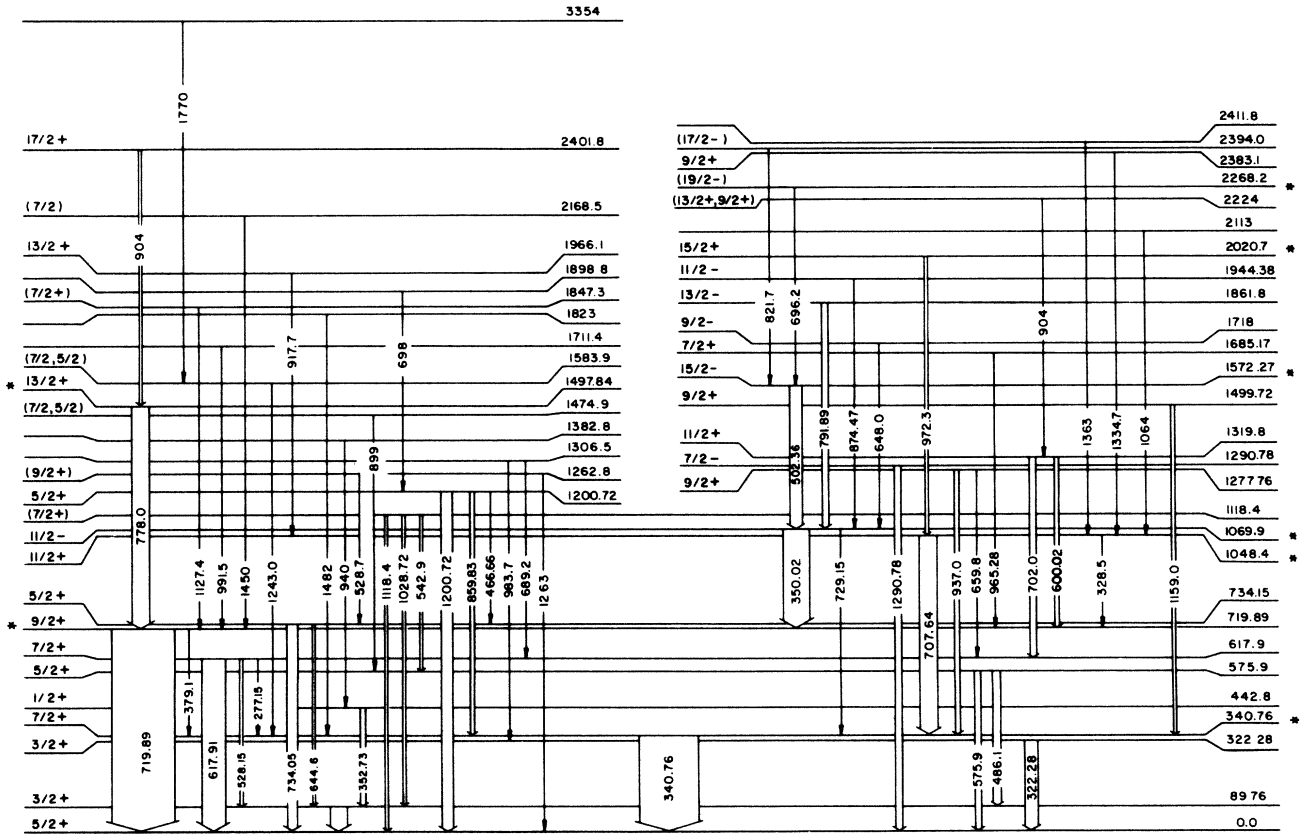

FIG. 5. Decay scheme for ^{99}Ru. Asterisks denote near-yrast states.

TABLE II. Analysis of γ rays emitted following the ^{98}Mo(^{3}He,2n)^{99}Ru reaction at 13 MeV.

Energy (keV)	$I_i^\pi - I_f^\pi$	Intensities ^{99}Ru	Intensities Other		A_{22} (Expt)	P_γ (Expt)	R_{DCOQ} (Expt)	α_2	δ	I_i (Ex. func)
89.76	$\frac{3}{2}^+ \rightarrow \frac{5}{2}^+$	310(8)								
277.15	$\frac{7}{2}^+ \rightarrow \frac{7}{2}^+$	30(10)	380(20)	^{197}Au			0.95(16)	0.5	−0.3 to +2	
322.28	$\frac{3}{2}^+ \rightarrow \frac{5}{2}^+$	230(5)	18(5)	^{99}Tc	−0.08(2)	−0.18(4)		0.8(2)	−0.01(2)	$\frac{3}{2}$
328.50	$\frac{11}{2}^+ \rightarrow \frac{9}{2}^+$	36(3)			−0.03(20)		1.1(2)	0.5(5)	0.17(2)	$\frac{11}{2}$
340.76	$\frac{7}{2}^+ \rightarrow \frac{5}{2}^+$	1000			−0.200(15)	−230(13)	1.5(1)	0.49(5)	−0.020(5)	$\frac{7}{2}$
350.02	$\frac{11}{2}^- \rightarrow \frac{9}{2}^+$	458(5)			−0.27(1)	+0.14(2)	1.6(1)	0.40(5)	−0.15(4)	$\frac{11}{2}$
352.73	$\frac{1}{2}^+ \rightarrow \frac{3}{2}^+$	111(3)			−0.06(5)	0.00(7)				$\frac{1}{2}, \frac{3}{2}$
379.13	$\frac{9}{2}^+ \rightarrow \frac{7}{2}^+$	29(3)			−0.04(13)	−0.31(18)		0.3(2)	0.7(3)	$\frac{9}{2}, \frac{7}{2}$
466.66	$\frac{5}{2}^+ \rightarrow \frac{9}{2}^+$	35(10)	430(10)	^{99}Tc						
486.14	$\frac{5}{2}^+ \rightarrow \frac{3}{2}^+$	160(5)	20(5)	^{99}Tc	−0.19(3)	−0.21(6)		0.4(1)	−0.02(3)	$\frac{5}{2}, \frac{3}{2}$
502.36	$\frac{15}{2}^- \rightarrow \frac{11}{2}^-$	220(5)			0.11(3)	0.32(6)				$\frac{15}{2}$
528.15	$\frac{7}{2}^+ \rightarrow \frac{3}{2}^+$	60(10)	230(10)	^{99}Tc						
528.7	$\frac{5}{2}^+$	22(5)								
542.9	$(\frac{7}{2}^+) \rightarrow \frac{5}{2}^+$	39(7)	51(10)	^{99}Tc						
575.90	$\frac{5}{2}^+ \rightarrow \frac{5}{2}^+$	96(10)	40(10)		0.01(4)	−0.02(8)		0.25(20)	−0.3(2)	$(\frac{5}{2}, \frac{3}{2})$
600.02	$\frac{7}{2}^+ \rightarrow \frac{9}{2}^+$	47(5)	31(5) 33(5)	^{98}Ru ^{99}Tc	0.02(8)	0.13(12)	1.5(3)	0.13(20)	0.8(5)	
617.91	$\frac{7}{2}^+ \rightarrow \frac{5}{2}^+$	410(5)			−0.39(2)	−0.07(3)		0.44(2)	−0.32(7)	$\frac{7}{2}$
644.64	$\frac{5}{2}^+ \rightarrow \frac{3}{2}^+$	62(3)								$\frac{5}{2}$
648.0	$\frac{9}{2}^- \rightarrow \frac{11}{2}^-$	48(5)	20(5)		0.28(15)	−0.16(14)	1.1(2)	0.45(20)	0.30(30)	$\frac{9}{2}$
659.8	$\frac{9}{2}^+ \rightarrow \frac{7}{2}^+$	25(5)	25(5)	LZ[a]	−0.27(9)	−0.24(14)	0.1(5)	0.5(2)	0.05(5)	
689.2	$\frac{7}{2}^+$	30(5)								
698.1	$\frac{5}{2}^+$	31(5)	217(10)							
702.00	$\frac{11}{2}^+ \rightarrow \frac{7}{2}^+$	102(5)			0.05(3)	0.15(10)		0.24(20)	0	$\frac{9}{2}, \frac{11}{2}$
707.64	$\frac{11}{2}^+ \rightarrow \frac{7}{2}^+$	310(5)			0.10(2)	0.25(6)	1.00(3)	0.22(7)		$\frac{11}{2}, \frac{9}{2}$
719.89	$\frac{9}{2}^+ \rightarrow \frac{5}{2}^+$	1093(5)			0.12(1)	0.17(2)		0.23(4)		$\frac{9}{2}$
729.15	$\frac{11}{2}^- \rightarrow \frac{7}{2}^+$	26(5)	510(5)	LZ[a]						
734.15	$\frac{5}{2}^+ \rightarrow \frac{5}{2}^+$	189(5)			0.05(3)	0.04(5)		0.15(17)	−1.8(1)	$\frac{3}{2}, \frac{5}{2}$
778.0[b]	$\frac{13}{2}^+ \rightarrow \frac{9}{2}^+$	290(15)	40(10) 90(10)	^{99}Tc ^{96}Mo						
791.89	$\frac{13}{2}^- \rightarrow \frac{11}{2}^-$	85(5)			0.35(5)	−0.7(2)		0.93(16)	0.18(12)	$\frac{13}{2}$
821.7	$\frac{17}{2}^- \rightarrow \frac{15}{2}^-$	14(3)	40(5)	^{99}Tc			3.0(15)	0.50	−1.2(7)	
859.83	$\frac{5}{2}^+ \rightarrow \frac{7}{2}^+$	69(5)			0.18(6)	−0.9(3)	1.2(2)	0.6(2)	−2.4(8)	$\frac{5}{2}$
874.47	$\frac{11}{2}^- \rightarrow \frac{11}{2}^-$	46(5)			−0.05(9)	0.02(26)	1.04(26)	0.3(2)	1.37(35)	$\frac{9}{2}, \frac{11}{2}$

TABLE II. (*Continued*).

Energy (keV)	$I_i^\pi - I_f^\pi$	Intensities ^{99}Ru	Intensities Other		A_{22} (Expt)	P_γ (Expt)	R_{DCOQ} (Expt)	α_2	δ	I_i (Ex. func)
899.0	$(\frac{7}{2},\frac{5}{2})\rightarrow\frac{5}{2}^+$	33(5)								$\frac{7}{2},\frac{5}{2}$
904.0[b]	$\frac{17}{2}^+\rightarrow\frac{13}{2}^+$	43(5)					0.93(13)			
904.0	$\frac{13}{2},\frac{9}{2}\rightarrow\frac{11}{2}^+$	30(5)					1.62(50)	0.5	<0.2	
917.7	$\frac{13}{2}^+\rightarrow\frac{11}{2}^+$	20(4)			0.26(21)	$-0.62(50)$	1.07(40)	0.6(2)	0.39(30)	$\frac{13}{2},\frac{15}{2}$
937.0	$\frac{9}{2}^+\rightarrow\frac{7}{2}^+$	79 (8)	667(10)	LZ[a]			2.2(4)	0.5	$-0.23(15)$	
940.0	$\frac{1}{2}^+$	8(3)	50(5)	^{99}Tc						
965.28	$\frac{7}{2}^+\rightarrow\frac{9}{2}^+$	34(4)			0.03(14)	$-0.8(3)$	1.2(4)	0.45(10)	-0.45	$\frac{5}{2},\frac{7}{2}$
972.3	$\frac{15}{2}^+\rightarrow\frac{11}{2}^+$	41(4)			0.23(12)	$+0.8(3)$	1.2(2)	0.6(3)	0	$\frac{15}{2}$
983.7	$\frac{3}{2}^+$	23(7)				0.5(5)				
991.5	$\frac{9}{2}^+$	16(3)	62(5)				2.0(13)			
1028.72	$(\frac{7}{2}^+)\rightarrow\frac{3}{2}^+$	40			0.18(13)					$\frac{7}{2},\frac{9}{2}$
1064.0	$\frac{11}{2}^+$	13(3)	55(5)	^{99}Tc						
1118.4	$(\frac{7}{2})^+\rightarrow\frac{5}{2}^+$	50(6)			$-0.07(7)$					$\frac{7}{2},\frac{9}{2}$
1127.4	$\frac{11}{2}^+\rightarrow\frac{9}{2}^+$	40(5)	15(5)	^{99}Tc	$-0.11(8)$	$-0.31(30)$	4.2(18)	0.35(10)	$-0.3(1)$	
1159.0	$\frac{9}{2}^+\rightarrow\frac{7}{2}^+$	47(5)			$-0.12(11)$	$-0.7(3)$	1.3(3)	0.25(10)	$-10(1)$	$(\frac{5}{2},\frac{7}{2},\frac{9}{2})$
1200.72	$\frac{5}{2}^+\rightarrow\frac{5}{2}^+$	190(5)			$-0.15(4)$	0.11(17)		0.39(20)	$-0.9(1)$	$\frac{5}{2}$
1243.0	$(\frac{7}{2},\frac{5}{2})\rightarrow\frac{7}{2}^+$	29(5)	14(5)	^{99}Tc			1.1(3)			$\frac{7}{2},\frac{5}{2}$
1263.0	$(\frac{9}{2}^+)\rightarrow\frac{5}{2}$	50(5)			$-0.17(10)$					$(\frac{9}{2})$
1290.78	$\frac{7}{2}^-\rightarrow\frac{5}{2}^+$	104(5)			$-0.23(10)$	$-0.3(6)$		0.6(2)	0	$\frac{5}{2},\frac{7}{2}$
1334.7[c]	$\frac{9}{2}\rightarrow\frac{11}{2}^+$	18(2)	200(5)	^{60}Co						$\frac{9}{2}$
1363.0	$\frac{11}{2}^+$	12(3)	10(3)	^{99}Tc						
1450.0	$(\frac{7}{2})\rightarrow\frac{9}{2}^+$	15(5)								$(\frac{7}{2})$
1482.0	$\frac{7}{2}^+$	13(5)	33(5)							
1770.	$(\frac{7}{2},\frac{5}{2})$	10(3)	34(5)							

[a]Background due to carbon and oxygen contamination of the target.
[b]The E2 character of this transition is seen in (α,xn) reactions.
[c]The spin assignment comes from the excitation-function measurement without the ^{60}Co source present.

analysis. Theoretical values of the DCOQ ratios must be calculated, however, for each hypothetical spin sequence and initial orientation, since the "typical" DCOQ values discussed in previous publications[11] are not applicable. Specific examples where the DCOQ gave extra information will be cited in the discussion of the level scheme.

V. THE LEVEL SCHEME

The level scheme deduced in the present work for ^{99}Ru is shown in Fig. 5. Several of the levels have been previously observed in $(\alpha xn,\gamma)$,[10,12,13] β-decay,[14] or Coulomb excitation reactions.[15] These levels are either at low excitation energies or near the yrast line. Our coincidence data have been used to establish many new levels. The placement of transitions in the level scheme was based not only on the existence of coincidences but consistency of intensities feeding and depopulating a proposed state. As usual there are many cases where two or more transitions have similar energies, and cannot be resolved in a singles measurement. These cases were identified by the comparison of singles and coincidence intensities. The transition intensities adopted were taken from singles measurements (specifically the A_{00} values of the angular distribution analysis) if the line was not contaminated. The proton-sort data was also helpful in that contamination from Tc isotopes could readily be identified. The intensity analysis is presented in Table II. As was mentioned earlier γ-ray energies can be determined in favorable cases with an accuracy of 50 eV. Accuracies of specific transitions listed in Table II are reflected by the number of significant figures.

Table II also includes results of the angular distribution, linear polarization, and DCOQ measurements. The A_{22} values tabulated are from fits with $A_{44}=0$. Where appropriate the initial spin from the excitation function analysis is given. Spins determined from the combined angular momentum analysis are listed. We feel that, unless indicated by parentheses, the spin assignments are given unambiguously from the procedure discussed above. Previously determined spins have been incorporated and/or verified as indicated.

A few placements and spin assignments require special attention. A 904.0-keV transition had been observed in previous work.[10] The previous data had shown this to be an E2 transition depopulating the $\frac{17}{2}^+$ 2401.1-keV state. Our coincidence data confirm this placement, but argue for a second "904"-keV transition feeding the 1320-keV state. Coincidences between a "904"-keV transition were observed with both the 702.0- and 600.02-keV transitions with intensities consistent with singles intensities. The previous authors also observed these coincidences, but postulated a 177.2-keV transition between their 1497.1- and 1319.8-keV states to explain them. They also remark that no coincidence with the 177.2-keV transition was observed, and suggest the possibility of a 904-keV doublet. In the present work no 177.2-keV coincidence was observed either. We also measure different DCOQ values for the two members of the 904 "doublet," consistent with one being a quadrupole and the second being predominantly a $|\Delta I| = 1$ dipole (see Table II). In fact based on our adopted intensities the conglomerate angular distribution should be isotropic, which agrees with our measurement [$A_{22}= 0.012 \pm (0.03)$]. The intensity of the second 904 relative to the quadrupole appears to be larger in our work than the previous work, which is to be expected considering the increased populations of non-yrast states.

The spin of the 1118.4-keV state is tentative. The existence of the level is established by coincidence data involving the 542.9-keV transition, which is contaminated. The suggested placement of the 1118.4- and 1028.8-keV transitions is based solely on energies. A spin of $\frac{7}{2}^+$ is consistent with our analysis, but since there is no way of checking contamination it must be tentative.

VI. DISCUSSION

The asterisks in Fig. 5 indicate near yrast states which constitute three bands built on $\frac{5}{2}^+$, $\frac{7}{2}^+$, and $\frac{11}{2}^-$ states. These states, and a few others, have been observed previously.[10,12–15] The large number of non-yrast states observed here exhibit a wide range of angular momenta from $\frac{1}{2}$ to $\frac{17}{2}$. The crucial question here is how many of the actual states present in ^{99}Ru have been populated. In a model independent way, one may count the number of states present and the expected spins by considering the coupling of an odd particle to various states of the core. In the extreme weak-coupling limit the coupling of an odd particle of spin j to a core state of spin **R** would result in a multiplet of levels with spins $|R-j| \leq I \leq R+j$ degenerate in energy at $E_I = E_R + E_j$. The actual particle-core interaction will of course remove this degeneracy and mix states from different multiplets to produce the actual nuclear states. Nevertheless, the number of states of a given I will remain unchanged. For a first-order estimate, it is also reasonable to consider only low-energy particle and core states. For this region the odd particle orbits expected at low energies are the $d_{5/2}$, $g_{7/2}$, and $h_{11/2}$. The pertinent excited states of the ^{98}Ru core are the 652-keV 2^+, the 1321-keV 0^+, the 1398-keV 4^+ and the 1415-keV 2^+ states.

The range of states expected is summarized in Table III, and compared to the number of states whose spins could be measured. All of the positive parity states could, in principle, lie in the experimental energy range, and candidates for most of them are observed. The most obvious deficit is for low-spin states. The only observed spin $\frac{1}{2}$ and $\frac{3}{2}$ states are at very low excitation energies where they may be populated indirectly. The comparison is not as favorable for negative parity states. The single particle $\frac{11}{2}^-$ energy is higher, so that many of the states might be expected at higher excitation energies. Candidates for multiplets corresponding to the lowest 0^+ and 2^+ states have been observed. This approach is certainly simplistic, and ignores the effects of other couplings. It does however seem that the reaction has been rather successful in populating an extensive set of the actual states present.

To do more than merely count states of a given spin, a model must be chosen. Ideally one would prefer a model which can include the coupling of all particles to all states of the core. The interacting boson-fermion approximation (IBFA) model[16] in fact does this, although its most exten-

TABLE III. Spins of expected states.

R	I										l_j
	$\frac{1}{2}$	$\frac{3}{2}$	$\frac{5}{2}$	$\frac{7}{2}$	$\frac{9}{2}$	$\frac{11}{2}$	$\frac{13}{2}$	$\frac{15}{2}$	$\frac{17}{2}$	$\frac{19}{2}$	
0,2,4	3	6	8	8	6	4	2	1			$d_{5/2}$,$g_{7/2}$
	(2)	2	5	7	5	3	2	1			Observed
0,2				2	2	4	2	2			$h_{11/2}$
				1	1	2	1	1			Observed

sively tested use has been for single-j calculations. ($j=\frac{11}{2}^-$ in this case). The authors of Ref. 13 have presented partial results of an IBFA calculation for ^{99}Ru, and demonstrated qualitative success in reproducing yrast energies. However in cases where several states of the same spin and parity are found at similar excitation energies, energy matches do not provide a definitive identification of states present, and transition properties become crucial. At present the IBFA cannot handle M1 transitions, which makes its use here of dubious value. The particle-rotor model has been used successfully to interpret other nuclei in this region.[17,18] It does not, of course, include all core states. For particles coupled to the "rotational" subset it can however calculate all transition properties in a straightforward fashion. For this reason the model chosen to interpret part of the observed Ru structure is a symmetric rotor plus particle model. The calculation of energies and wave functions is the same as that used by Smith and Rickey for Pd nuclei.[17] The calculation of electromagnetic transition properties, branching ratios, multipole mixing ratios and lifetimes, is the same used by Popli *et al.* in interpreting Ag nuclei.[18]

Even though the core angular momentum is not a good quantum number, all the calculated wave functions exhibit a dominant R value. By inspecting the wave functions and grouping the states which have the same dominant single particle parentage and R value, multiplets can be identified.

The specific model utilizes a rotational Hamiltonian in the strong-coupling limit modified to include a variable moment-of-inertia. The basis states are thus rotational states built on Nilsson single-particle states,[19] characterized by good K and Ω, the projection of the total angular momentum I and the particle angular momentum j on the symmetry axis, respectively. Pairing is treated by the Bardeen-Cooper-Schrieffer (BCS) formalism. The Coriolis and recoil terms, which mix these states, are treated exactly.

The Nilsson calculation was performed using the parameter $\mu=0.350$ and $\kappa=0.064$, which gave the closest agreement with the levels at zero deformation as listed by Reehal and Sorenson.[20] The resultant Nilsson diagram is shown in Fig. 6. A deformation of $\delta=0.12$ was selected. At this deformation the Fermi level should lie between the $\frac{3}{2}^+[422]$ and $\frac{1}{2}^+[420]$ levels. The empirical results of Bohr and Mottelson[21] suggest a pairing gap of 1.1 MeV. In the resultant calculation the Fermi level was varied slightly to obtain the best energy fit for near-yrast states. Fermi levels of $N=46.35$ MeV for $N=4$ states and 46.30 MeV for $N=5$ states were adopted. The VMI inertial parameters[22] used in the calculations were $\mathcal{I}_0=0$ for both shells, and $C=0.065$ or 0.035 MeV^3 for $N=4$ and $N=5$ shells, respectively. Coriolis and recoil matrix elements were attenuated by a factor of 0.8. In the transition probability calculations collective effects for E2 transition are treated by calculating an effective quadrupole moment of the core. For this the deformation δ was considered a free parameter, since the wave functions are insensitive to small changes in δ. The best results were obtained with $\delta=0.12$ for positive parity states and $\delta=0.10$ for negative parities.

In establishing the correspondence between experimental and calculated states the following criteria were used. First the energy comparison must be sensible. No attempts were made to fine-tune energies in the calculation, since this would increase the number of free parameters. Thus while the overall agreement between calculated and observed energies is good, it is not adequate for a definitive identification in many cases. As an example the model predicts two low-lying $\frac{3}{2}^+$ states differing in energy by $\sim$200 keV. However in the calculation the order of these two states can be exchanged by small parameter variations. The predicted wave functions are quite distinct, and are relatively insensitive to the same parameter changes. Thus the electromagnetic decay properties are a more characteristic signature of the model wave functions. The second criterion of comparing predicted and observed branching ratios thus provides a more reliable identification. Correspondence of branching ratios means that not only does the observed state decay as predicted, but is fed as predicted.

For each observed state, candidates from the calculation were first selected based on their energies. Using experimental energies, branching ratios for the decay of each candidate were calculated. When a match was found the established correspondence was then used later in investigating the decay of higher-lying states. If no match was found the observed state was assumed to be nonrotational. The states for which no spin could be determined were compared to a variety of calculated states to see if any correspondence was possible.

The results of this analysis are given in Table IV. The states are grouped into multiplets, based on the dominant R and j of the calculated wave functions. The calculated energies have been normalized, since the calculation does not return absolute energies. The independent positive and negative parity calculations have been normalized to give the $\frac{5}{2}^+$ ground state zero energy, and place the lowest negative parity state ($\frac{11}{2}^-$) at the correct energy. We have observed that all states with $g_{7/2}$ parentage seem

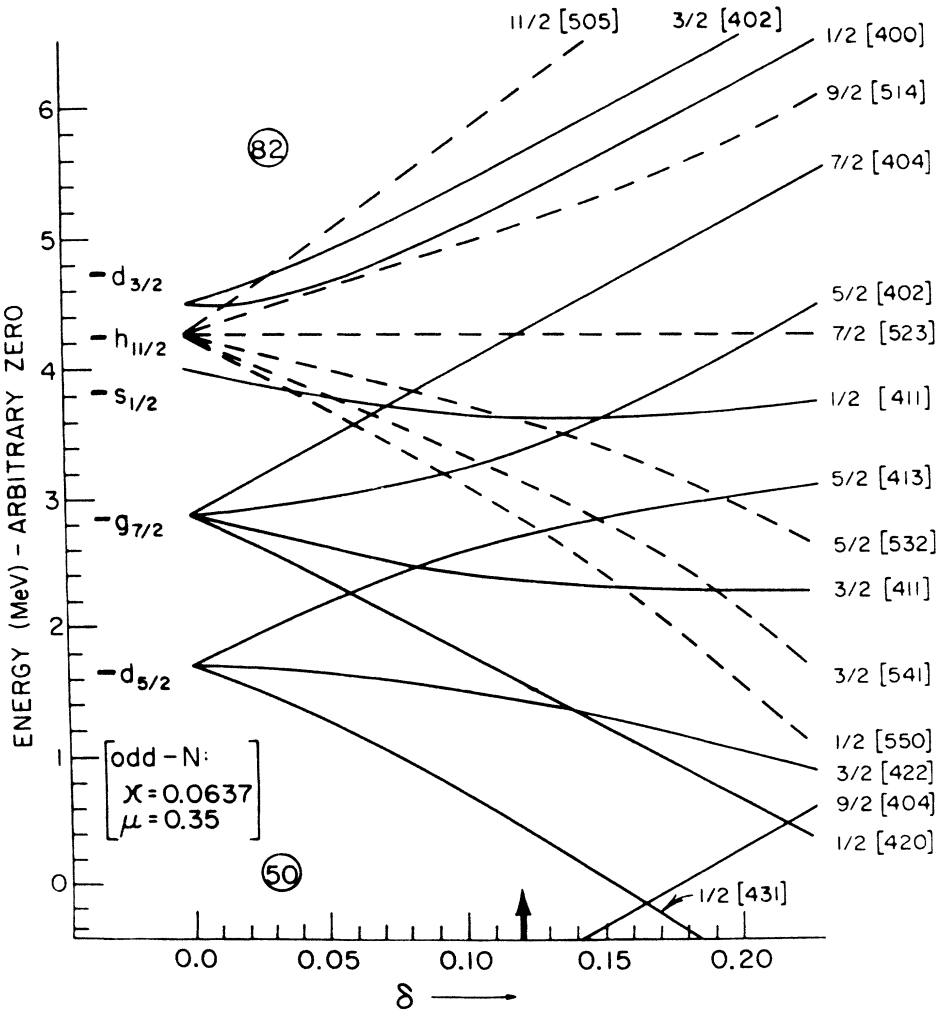

FIG. 6. Nilsson diagram for odd neutrons in ^{99}Ru.

to be shifted down in energy relative to those of $d_{5/2}$ parentage by about 200 keV. Thus we have arbitrarily renormalized all "$g_{7/2}$ energies" to set the lowest $\frac{7}{2}^+$ state at the experimental energy of 341 keV. Finally a systematic trend to overestimate higher spin yrast states has been observed. This is due to limitations of the VMI formalism, even though it is superior to a fixed moment of inertia. Thus for each multiplet all energies have been shifted by a small amount to emphasize the trends within the multiplet. This effect is given in parentheses below the calculated energies for the yrast state of each multiplet. There are three states included as tentative members of multiplets where spin could not be measured, but whose decay pattern and energies match the calculation. The assumed spins are enclosed in square brackets. Finally three states are included, labeled with asterisks, which were not observed in the present work. These have been singled out to facilitate the identification of "nonrotational" states.

In this interpretation several features of the reaction can be identified. The comparison indicates that all members of the three multiplets obtained by coupling $d_{5/2}$, $g_{7/2}$, and $h_{11/2}$ neutrons to the first 2^+ state of the core have been populated. Thus at the lower excitation energies involved the reaction has been successful in populating non-yrast states. Multiplets based on the $R=4$ core excitation might be expected to present a more severe challenge, since they should lie at higher excitation energies. There are candidates for a complete $R=4d_{5/2}$ multiplet. The spin of the state tentatively assigned as the $\frac{3}{2}^+$ member could not be measured, yet its branching ratio and energy agree nicely with those calculated. Purely on the basis of energy this state would be expected to decay to the ground state since it does decay to $\frac{3}{2}^+$ and $\frac{7}{2}$ states. The absence of the ground state branch is thus a specific signature. Candidates for five of the eight members of the $R=4g_{7/2}$ multiplet were observed. Again the spins of two states, the projected $\frac{11}{2}^+$ and $\frac{7}{2}^+$ members, could not be measured. They are simply the only states observed at approximately the right energies that decay as predicted. Candidates for the lower spin members were not observed. None of the unassigned states have the predicted decay properties. The calculated energies of these low-spin states were higher than any observed states of corresponding spins, implying a spin cutoff as a function of energy for the reaction. That is, as the

TABLE IV. Multiplet association.

	E_i (keV)		E_γ (keV)	I_i^π	I_f^π	Branching ratio		l_j
	Expt	Theor				Expt	Theor	
$R=0$								
	0	≡0		$\frac{5}{2}^+$				$d_{5/2}$
	340.76	≡341	341	$\frac{7}{2}^+$	$\frac{5}{2}^+$	1.00	0.999	$g_{7/2}$
			251		$\frac{3}{2}^+$	0.00	0.001	
	1069.91	≡1070	729	$\frac{11}{2}^-$	$\frac{7}{2}^+$	0.06	0.00	$h_{11/2}$
			350		$\frac{9}{2}^+$	0.94	1.00	
$R=2$								
	719.89	720	720	$\frac{9}{2}^+$	$\frac{5}{2}^+$	0.96	0.76	$d_{5/2}$
		(−24)	379		$\frac{7}{2}^+$	0.02	0.18	
			144		$\frac{5}{2}^+$	0.00	0.00	
			102		$\frac{7}{2}^+$	0.02	0.06	
	617.91	605	618	$\frac{7}{2}^+$	$\frac{5}{2}^+$	0.73	0.74	$d_{5/2}$
			528		$\frac{3}{2}^+$	0.20	0.20	
			278		$\frac{7}{2}^+$	0.07	0.06	
	734.15	784	734	$\frac{5}{2}^+$	$\frac{5}{2}^+$	0.75	0.82	$d_{5/2}$
			644		$\frac{3}{2}^+$	0.25	0.18	
	89.76	197	90	$\frac{3}{2}^+$	$\frac{5}{2}^+$	1.00	1.00	$d_{5/2}$
	442.8	402	353	$\frac{1}{2}^+$	$\frac{3}{2}^+$	1.00	0.99	$d_{5/2}$
			443		$\frac{5}{2}^+$	0.00	0.01	
	1048.4	1048	708	$\frac{11}{2}^+$	$\frac{7}{2}^+$	0.92	0.99	$g_{7/2}$
		(−54)	327		$\frac{9}{2}^+$	0.08	0.01	
			431		$\frac{7}{2}^+$	0.00	0.00	
	1277.76	1299	1278	$\frac{9}{2}^+$	$\frac{5}{2}^+$	0.00	0.04	$g_{7/2}$
			937		$\frac{7}{2}^+$	0.75	0.70	
			660		$\frac{7}{2}^+$	0.25	0.20	
			560		$\frac{9}{2}^+$	0.00	0.06	
	1685.17	1612	1067	$\frac{7}{2}^+$	$\frac{7}{2}^+$	0.00	0.00	$g_{7/2}$
			965		$\frac{9}{2}^+$	1.00	0.87	
			1345		$\frac{7}{2}^+$	0.00	0.13	
	575.9	727	576	$\frac{5}{2}^+$	$\frac{5}{2}^+$	0.43	0.50	$g_{7/2}$
			486		$\frac{3}{2}^+$	0.57	0.50	
			235		$\frac{7}{2}^+$	0.00	0.001	
	322.28	241	322	$\frac{3}{2}^+$	$\frac{5}{2}^+$	1.00	0.96	$g_{7/2}$
			232		$\frac{3}{2}^+$	0.00	0.04	
	1572.27	1572	503	$\frac{15}{2}^-$	$\frac{11}{2}^-$	1.00	1.00	$h_{11/2}$
		(+7)						
	1861.8	1952	813	$\frac{13}{2}^-$	$\frac{11}{2}^+$	0.00	0.01	$h_{11/2}$
			792		$\frac{11}{2}^-$	1.00	0.87	
			289		$\frac{15}{2}^-$	0.00	0.12	
	1944.38	2280	896	$\frac{11}{2}^-$	$\frac{11}{2}^+$	0.00	0.01	$h_{11/2}$
			874		$\frac{11}{2}^-$	1.00	0.99	
	1718.	1587	1379	$\frac{9}{2}^-$	$\frac{7}{2}^+$	0.00	0.05	$h_{11/2}$
			999		$\frac{9}{2}^+$	0.00	0.01	
			671		$\frac{11}{2}^+$	0.00	0.00	
			649		$\frac{11}{2}^-$	1.00	0.94	
	1290.78	1105	1291	$\frac{7}{2}^-$	$\frac{5}{2}^+$	1.00	0.99	$h_{11/2}$
			950		$\frac{7}{2}^+$	0.00	0.00	
			220		$\frac{11}{2}^-$	0.00	0.01	

TABLE IV. (*Continued*).

	E_i (keV)		E_γ (keV)	I_i^π	I_f^π	Branching ratio		l_j
	Expt	Theor				Expt	Theor	
$R=4$								
	1497.84	1498	778	$\frac{13}{2}^+$	$\frac{9}{2}^+$	1.00	0.93	$d_{5/2}$
		(−400)	449		$\frac{11}{2}^+$	0.00	0.07	
	1319.8	1351	702	$\frac{11}{2}^+$	$\frac{7}{2}^+$	0.65	0.65	$d_{5/2}$
			600		$\frac{9}{2}^+$	0.35	0.32	
			979		$\frac{7}{2}^+$	0.00	0.00	
			271		$\frac{11}{2}^+$	0.00	0.03	
	1499.72	1500	1159	$\frac{9}{2}^+$	$\frac{7}{2}^+$	1.00	0.84	$d_{5/2}$
			780		$\frac{9}{2}^+$	0.00	0.16	
	1118.4	1342	1118	$(\frac{7}{2}^+)$	$\frac{5}{2}^+$	0.38	0.49	$d_{5/2}$
			1029		$\frac{3}{2}^+$	0.31	0.21	
			543		$\frac{5}{2}^+$	0.31	0.30	
	1200.72	1030	1201	$\frac{5}{2}^+$	$\frac{5}{2}^+$	0.64	0.89	$d_{5/2}$
			860		$\frac{7}{2}^+$	0.23	0.10	
			625		$\frac{5}{2}^+$	0.00	0.00	
			467		$\frac{5}{2}^+$	0.13	0.01	
	1306.5	1389	984	$[\frac{3}{2}^+]$	$\frac{3}{2}^+$	0.68	0.90	$d_{5/2}$
			966		$\frac{7}{2}^+$	0.00	0.00	
			689		$\frac{7}{2}^+$	0.32	0.10	
	2020.7	2024	972	$\frac{15}{2}^+$	$\frac{11}{2}^+$	1.00	1.00	$g_{7/2}$
		(−250)						
	2224	2200	904	$(\frac{13}{2}^+)$	$\frac{11}{2}^+$	1.00	0.86	$g_{7/2}$
			1175		$\frac{11}{2}^+$	0.00	0.14	
	2411.8	2363	1363	$[\frac{11}{2}^+]$	$\frac{11}{2}^+$	1.00	0.98	$g_{7/2}$
			1092		$\frac{11}{2}^+$	0.00	0.00	
			911		$\frac{9}{2}^+$	0.00	0.02	
	2383.1	2391	1335	$\frac{9}{2}^+$	$\frac{11}{2}^+$	1.00	0.66	$g_{7/2}$
			1663		$\frac{9}{2}^+$	0.00	0.20	
			883		$\frac{9}{2}^+$	0.00	0.02	
			1765		$\frac{7}{2}^+$	0.00	0.10	
			2042		$\frac{7}{2}^+$	0.00	0.04	
	2113	2404	1064	$[\frac{7}{2}^+]$	$\frac{11}{2}^+$	1.00	0.80	$g_{7/2}$
			1393		$\frac{9}{2}^+$	0.00	0.00	
			1495		$\frac{7}{2}^+$	0.00	0.00	
			1772		$\frac{7}{2}^+$	0.00	0.20	
	1292.1[a]	1382	1292	$(\frac{3}{2}^+)$	$\frac{5}{2}^+$	1.00	0.75	$g_{7/2}$
			1202		$\frac{3}{2}^+$	0.00	0.22	
			970		$\frac{3}{2}^+$	0.00	0.01	
			750		$\frac{1}{2}^+$	0.00	0.01	
	617.5[a]	762	618	$\frac{1}{2}^+$	$\frac{5}{2}^+$	0.10	0.00	$g_{7/2}$
			528		$\frac{3}{2}^+$	0.85	0.97	
			296		$\frac{3}{2}^+$	0.02	0.01	
			175		$\frac{1}{2}^+$	0.03	0.02	
	2268.2	2268	697	$(\frac{19}{2}^-)$	$\frac{15}{2}^-$	1.00	1.00	$h_{11/2}$
		(−100)						
	2394.0	2613	821	$(\frac{17}{2}^-)$	$\frac{15}{2}^-$	1.00	0.96	$h_{11/2}$
			533		$\frac{13}{2}^-$	0.00	0.02	
			126		$\frac{19}{2}^-$	0.00	0.02	

TABLE IV. (*Continued*).

	E_i (keV)		E_γ (keV)	I_i^π	I_f^π	Branching ratio		l_j
	Expt	Theor				Expt	Theor	
$R=6$								
	2401.8	2402	904	$\frac{17}{2}^+$	$\frac{13}{2}^+$	1.00	1.00	$d_{5/2}$
Unassigned states from the present work								
	1262.8		1263	$(\frac{9}{2}^+)$	$\frac{5}{2}^+$	0.72		
			529		$\frac{5}{2}^+$	0.28		
	1383		940		$\frac{1}{2}^+$	1.00		
	1474.9		899		$\frac{5}{2}^+$	1.00		
	1583.9		1243	$(\frac{7}{2},\frac{5}{2})$	$\frac{7}{2}^+$	1.00		
	1711.4		992		$\frac{9}{2}^+$	1.0		
	1847.3		1127	$(\frac{7}{2}^+)$	$\frac{9}{2}^+$	1.00		
	1898.8		698		$\frac{5}{2}^+$	1.00		
	1966.1		918	$\frac{13}{2}^+$	$\frac{11}{2}^+$	1.00		
	2168.5		1449	$(\frac{7}{2}^+)$	$\frac{9}{2}^+$	1.00		
	3354		1770	$(\frac{7}{2}),(\frac{5}{2})$		1.00		
States observed in other work								
	850.3			$(\frac{1}{2}^+,\frac{3}{2}^+)$				
	897.2			$(\frac{1}{2}^+,\frac{3}{2}^+)$				
	1000.2	1085	1000	$(\frac{3}{2}^+)$	$\frac{5}{2}^+$	0.94	0.79	$s_{1/2}$
			911		$\frac{3}{2}^+$	0.06	0.21	
	1382.9			$(\frac{1}{2}^+,\frac{3}{2}^+)$				
	1505.1			$(\frac{1}{2}^+,\frac{3}{2}^+)$				
	1532.9			$(\frac{1}{2}^+,\frac{3}{2}^+)$				
	1662.1	1554	1662	$(\frac{1}{2}^+)$	$\frac{5}{2}^+$	0.15	0.13	$s_{1/2}^b$
			1572		$\frac{3}{2}^+$	0.85	0.87	
	1749.			$(\frac{1}{2}^+,\frac{3}{2}^+)$				

[a] State not observed in the present work, but observed in β-decay.

[b] The experimental branching ratios for this state are calculated using the two observed transitions to states included in the model. A third transition was observed experimentally.

excitation energy increases, the population of low-spin states far off the yrast line decreases. One must ask whether the calculated energies of these states mean anything. Low-spin states in ^{99}Ru have been studied previously via the β-decay of ^{99}Rh.[14] Direct β^+ feedings from the parent $\frac{1}{2}^-$ state were observed to several states with logft values characteristic of first-forbidden transitions, implying spins $\frac{1}{2}^+$ or $\frac{3}{2}^+$. The lowest of these states at 617.5 keV has been assigned a spin of $\frac{1}{2}^+$, and has the correct decay properties to be the $\frac{1}{2}^+$ of this $g_{7/2}$ multiplet. On the same grounds the state of 1292.1 keV is a candidate for the $\frac{3}{2}^+$ member. These have been included in Table IV to indicate that while they were not populated in the present work their location may be known. Only two states, the highest spin $\frac{19}{2}^-$ and $\frac{17}{2}^-$ levels, of the $R=4h_{11/2}$ multiplet were observed. This multiplet should lie at still higher excitation energies, and so this general trend continues. We surmise that the reaction can populate the complete set of existing states as long as they lie in an excitation range small compared to the initial excitation energy in the final nucleus, but this completeness deteriorates at higher excitation energies.

Ten states were observed which cannot be associated with these "rotational" multiplets. They decay to positive parity states only, and thus are likely to be positive parity states. The spin information on these states is sketchy. The unknown spins are likely to be greater than $\frac{3}{2}^+$ considering their excitation energies.

Eight additional states were observed in β-decay with logft values suggesting spins of $\frac{1}{2}^+$ or $\frac{3}{2}^+$. The total group of states from both experiments is a candidate for other particle-core couplings. Rotational couplings not considered yet involve $s_{1/2}$ and $d_{3/2}$ particles. The calculation suggests that states involving the $d_{3/2}$ particle should lie above 3 MeV. There are however states predicted in the observed energy range representing coupling of the $s_{1/2}$ particle to the lowest 0^+ and 2^+ states. If the 1662.1- and 1000.2-keV states (β-decay) have spins $\frac{1}{2}^+$ and $\frac{3}{2}^+$, respectively, they are candidates for $s_{1/2}$ couplings based on their energies and branching ratios.

The remaining sixteen states must be left as candidates for particle coupled to "non-rotational" states.

VII. ROTATIONAL SYSTEMATICS

In previous work where the particle-rotor model has been used to describe yrast bands, much has been said about the systematic effects the position of the Fermi surface has on the band structure.[17,18] Simply stated, as the Fermi surface moves from low Ω to high Ω, the resulting yrast band changes from decoupled to strong coupled. The position of the Fermi surface affects the systematics of non-yrast states as well.

The concept of particle-core multiplets is not appropriate for highly-deformed nuclei where the strong coupling limit is a good approximation. The Coriolis interaction, which tries to decouple the particle from the core, can make the multiplet picture a more natural one. When the Coriolis interaction mixes states of the same spin but different Ω, it tends to produce states with a dominant R component, and to depress in energy those states with small R relative to those with large R. In slightly deformed nuclei the effects of the Coriolis interaction can be large. The single-j case, negative parity states in ^{99}Ru, is conceptually the simplest, although the same arguments hold for mixed-j shells. Coriolis matrix elements depend on the terms $(I-K)$ and $(j-\Omega)$. Thus the matrix elements can be largest for low K or Ω and high I or j. In the ^{99}Ru calculation the relevant matrix elements are large enough to ensure that the final states of a given spin are ordered in energy by their dominant R values. For example the members of the $R=2$, $j=\frac{11}{2}$ multiplet are the lowest negative parity states of each spin except for the $I=j$ member, which is the second $\frac{11}{2}^-$ state.

The relative energies of different members of a multiplet are systematically sensitive to the position of the Fermi surface. In the particle rotor model low spin states can come only from basis states of low Ω values, since I must be greater than or equal to Ω. When the Fermi surface is near (or below) the lowest Ω values, low spin states lie at low excitation energies in the basis, with higher spins lying at successively higher energies. The Coriolis interaction acts on all states, depressing them in energy, with its largest effects on high spin states. Thus stepping from low to high spin the final energy first increases to the $I=j$ state, and then decreases. The result is a characteristic skewed arch peaking at the $I=j$ state, with the antialigned states lying below the aligned states. As the Fermi surface is moved up through higher Ω values, low spin states must also move up relative to the high spin states in the basis. Although the Coriolis interaction depresses them in energy, they are found at higher energies (relative to the $I=j$ state) than in the low Ω case. In addition the higher spin states systematically become weighted toward higher Ω. Thus the Coriolis matrix elements decrease,

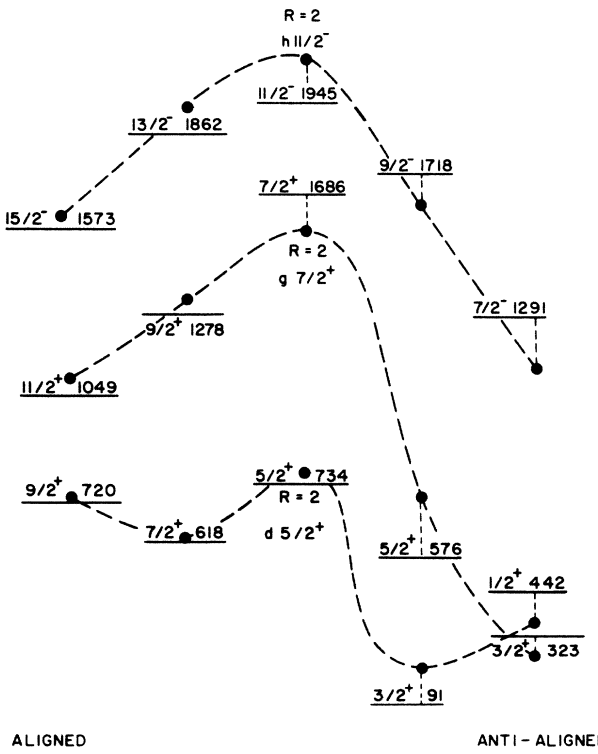

FIG. 7. States identified as members of the $R=2$ multiplets based on $d_{5/2}$, $g_{7/2}$, and $h_{11/2}$ particles. Horizontal lines represent experimental states. Dots represent the calculated energies, and are connected with dashed curves.

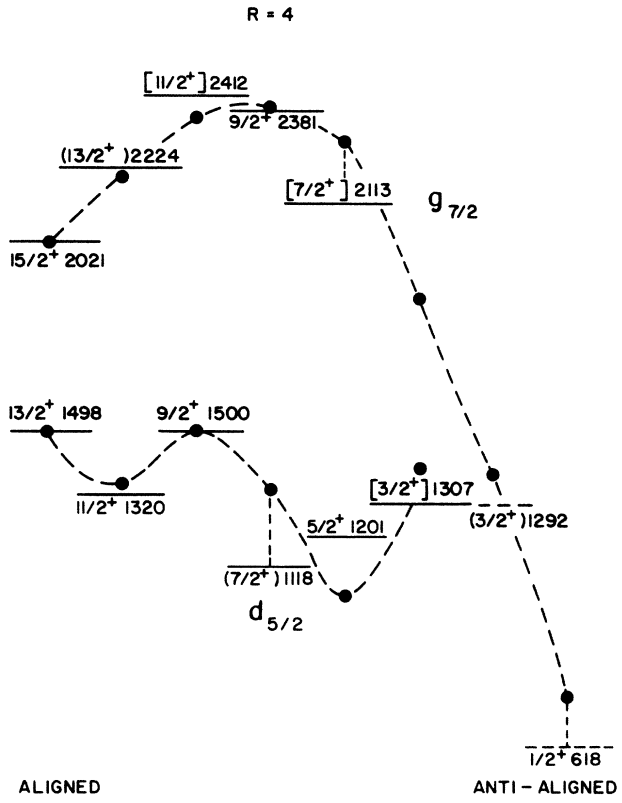

FIG. 8. States identified as members of the $R=4$ multiplets based on $d_{5/2}$ and $g_{7/2}$ particles. Spins in brackets have not been measured, and are based solely on the correspondence of experimental energies and branching ratios to those calculated. The dashed curves connect the calculated energies shown as dots.

and the higher spin states are depressed by smaller amounts. The resultant multiplet thus flattens out.

As was mentioned earlier, in ^{99}Ru the Fermi surface lies between the $\frac{3}{2}^+$[422] and $\frac{1}{2}^+$[420] Nilsson states. This places it below all the $g_{7/2}$ and $h_{11/2}$ orbits, but well up in the $d_{5/2}$ orbits. Thus one would expect the characteristic arched multiplets for $g_{7/2}$ and $h_{11/2}$ multiplets, but flatter $d_{5/2}$ multiplets. Figure 7 compares the experimental and calculated multiplets for $R=2$ multiplets, and Fig. 8 presents the $R=4$ comparison. The expected trends are clearly seen. The staggering seen in $d_{5/2}$ multiplets is remarkably well reproduced. This is in fact due to the details of the calculation for the mixed-j shell.

VIII. CONCLUSIONS

The present work demonstrates that the (^{3}He,2nγ) reaction is a powerful tool for populating non-yrast states with a wide range of angular momenta. In fact a model-independent count indicates that most of the states expected at low energies have populated. The small orientation of the final system relative to that following (HI,xnγ) reactions presents problems in making spin assignments, but these problems can be overcome by utilizing linear-polarization and excitation-function measurements in addition to the standard angular-distribution analysis.

A large subset of the observed states have both the energies and decay properties predicted by a simple particle-rotor model. In this interpretation four complete particle-core multiplets have been observed, three where the first $R=2$ core excitation is coupled to $d_{5/2}$, $g_{7/2}$, and $h_{11/2}$ particles, and one for the $R=4d_{5/2}$ coupling. The higher-spin members for an $R=4g_{7/2}$ multiplet may have been observed. Additional low-spin states predicted agree with those populated in β-decay. A group of states have been observed which do not correspond to any predicted. We suggest that these states involve couplings to the second $R=0$ and 2 states of the core, which are not included in the model.

This work was partially supported by the National Science Foundation.

*Present address: Department of Physics and Astronomy, University of South Carolina, Columbia, SC 29208.

†Present address: Department of Physics, Kansas State University, Manhattan, KS 66506.

‡Present address: Los Alamos Scientific Laboratory, Los Alamos NM 87544.

[1]C.S. Whisnant, R.H. Castain, F.A. Rickey, and P.C. Simms, Phys. Rev. Lett. **50**, 724 (1983).

[2]R.H. Castain, F.A. Rickey, and P.C. Simms (unpublished).

[3]Rakesh Popli, F.A. Rickey, L.E. Samuelson, and P.C. Simms, Phys. Rev. C **23**, 1085 (1981).

[4]F.A. Rickey, J.A. Grau, L.E. Samuelson, and P.C. Simms, Phys. Rev. C **15**, 1530 (1977).

[5]T. Yamazaki, Nucl. Data **A3**, 1 (1967).

[6]K.S. Krane, Nucl. Instrum. Methods **98**, 205 (1972).

[7]K.S. Krane and R.M. Steffen, Phys. Rev. C **2**, 724 (1970).

[8]P. Taras, Can. J. Phys. **49**, 328 (1971).

[9]Jin Soon Kim, Y.K. Lee, K.A. Hardy, P.C. Simms, J.A. Grau, G.J. Smith, and F.A. Rickey, Phys. Rev. C **12**, 499 (1975).

[10]G. Kajrys, R. Lecomte, S. Landsberger, and S. Manaro, Phys. Rev. C **28**, 1504 (1983).

[11]J.A. Grau, L.E. Samuelson, F.A. Rickey, P.C. Simms, and G.J. Smith, Phys. Rev. C **14**, 2297 (1976).

[12]C.M. Lederer, J.M. Jaklevic, and J.M. Hollander, Nucl. Phys. **A169**, 489 (1971).

[13]E.H. du Marchie van Voorthuysen, M.J.A. de Voigt, N. Blasi, and J.F.W. Jansen, Nucl. Phys. **A355**, 93 (1981).

[14]L.R. Medsker, L.H. Fry, Jr., and J.L. Yntema, Phys. Rev. C **15**, 649 (1977).

[15]O.C. Kistner and A. Schwarzschild, Phys. Rev. **154**, 1182 (1967).

[16]F. Iachello and O. Scholten, Phys. Rev. Lett. **43**, 679 (1979).

[17]H.A. Smith, Jr. and F.A. Rickey, Phys. Rev. C **14**, 1946 (1976).

[18]Rakesh Popli, J.A. Grau, S.I. Popik, L.E. Samuelson, F.A. Rickey, and P.C. Simms, Phys. Rev. C **20**, 1350 (1979).

[19]S.G. Nilsson, K. Dan. Vidensk. Selsk. Mat.-Fys. Medd. **29**, No. 16 (1955).

[20]B. Reehal and R. Sorensen, Phys. Rev. C **2**, 819 (1970).

[21]A. Bohr and B. Mottelson, *Nuclear Structure* (Benjamin, New York, 1969), Vol.1, p.169.

[22]M.A. J. Mariscotti, G. Scharff-Goldhaber, and B. Buck, Phys. Rev. **178**, 1864 (1969).